# Acta Crystallographica Section D

**Volume 70 (2014)**

**Supporting information for article:**


## Structure and mechanism of a nonhaem-iron SAM-dependent *C*-methyltransferase and its engineering to a hydratase and *O*-methyltransferase

**Xiao-Wei Zou, Yu-Chen Liu, Ning-Shian Hsu, Chuen-Jiuan Huang, Syue-Yi Lyu, Hsiu-Chien Chan, Chin-Yuan Chang, Hsien-Wei Yeh, Kuan-Hung Lin, Chang-Jer Wu, Ming-Daw Tsai and Tsung-Lin Li**

## S1. Supporting methods

### S1.1. Enzymatic reaction

A typical enzymatic assay for methyltransferase activity was conducted in a buffer solution of 150 µl for 4.5 hr at 25°C, wherein it contained enzyme (2.5 ng), PBS (50 mM, pH 7.4), Ppy (3 mM), and SAM (1.5 mM). After incubation, the reaction mixture was centrifuged at 16000 g for 5 min and then filtered with an ultracentrifugal membrane with 5 kDa cut-off (Millipore). The resulting filtrate was subjected to HPLC-ESI/MS analysis in a gradient solvent system: acetonitrile linearly increased from 0 to 60% against water (0.1% TFA) in 30 min. On-line LC-ESI/MS spectra were recorded by an Agilent HPLC 1200 series instrument coupled with a Thermo-Finnigan LTQ-XL ESI-ion trap mass spectrometer in a positive mode. For non-heme oxygenase activity assay, MppJ was purified in a reducing environment, which contained pre-degased buffer 50 mM HEPES pH 8.0 and 5 mM DTT. Then Enzyme (10 ng) was incubated with 10 mM Ppy or 4HPpy in the presence of 1 mM ascorbic acid (a reducing agent). Reactions were performed at 25°C for overnight incubation. After incubation, enzyme was quenched by adding 6N HCl. The protein was removed by centrifugation and the resultant was subjected to LC/MS analysis.

### S1.2. Site-directed mutagenesis

Site-directed mutagenesis was carried out using QuickChange (Stratagene). The wild-type MppJ was used as the template for single mutation. For multiple mutations, the single or double mutant was used as the template. All mutations were confirmed by DNA sequencing. The pET/His plasmid was used for protein expression. Mutant enzymes were purified with the same protocol for the wild-type MppJ.

### S1.3. Analytical ultracentrifugation analysis

The sedimentation velocity experiments were performed with a Beckman-Coulter XL-I analytical ultracentrifuge. Samples and buffers were loaded into 12 mm standard double-sector Epon charcoal-filled centerpieces and mounted in an An-60 Ti rotor. 400 µl of 1 mg $ml^{-1}$ protein sample were loaded into the cell. Sedimentation velocity experiments were performed at a rotor speed of 42,000 r.p.m. at 20°C. The signals of samples were monitored at 280 nm and collected every 3 min for 6 hr. The raw data of experiments were calculated using SedFit (Schuck, 2000) software. The density and viscosity of buffer were calculated using Sednterp software (http:// www.jphilo.mailway.com/default.htm). All samples were visually checked for clarity after ultracentrifugation.

### S1.4. Isothermal titration calorimetry analysis

ITC experiments were performed at 25°C using an iTC200 microcalorimeter (MicroCal Inc.; Northampton, MA). All the samples were dissolved in 50 mM HEPES buffer solutions (pH 8.0). The titration consisted of 15 injections of 2 μl in 150 s intervals. Each titration contained 0.1 mM MppJ in the sample cell (250 μl). Forty microliter of SAM, Ppy, or SAH (1 mM) were loaded in the injection syringe. The reference cell was filled with water for all experiments. The heat of dilution was determined by titrating the substrates into the buffer without enzyme and subtracted prior to curve fitting. Data analysis was performed by using the Origin 7.0 software provided by MicroCal.

### S1.5. X-ray absorption spectroscopy

X-ray absorption spectra were recorded at beamline 17C1 at the National Synchrotron Radiation Research Center (Taiwan). Two millimolar of MppJ in a buffer solution (50 mM HEPES, pH 8.0) were used in data collection. A cold-air device was set at 10°C for avoiding photodamage. The absorption spectra were collected in fluorescence mode with solid-state detector or Lytle detector. The first inflection point at 7112 eV of Fe foil spectrum was used for energy calibration. Raw X-ray absorption data were analyzed following the standard procedure, including background subtractions and normalization. Data were processed by using ATHENA (Ravel & Newville, 2005) software.

### S1.6. Electron paramagnetic resonance spectroscopy

EPR spectra were recorded at the X band (9.5 GHz) by using a Bruker X-band E500CW spectrometer (Bruker Biospin). Two millimolar samples were loaded into an EPR sample tube and immersed into a liquid nitrogen Cold Finger Dewar to maintain the temperature at 77K for data collection.

### S1.7. Chiral HPLC analysis

A Phenomenex Chirex (D)-penicillamine phase 3126 (4.6 mm × 250 mm) ligand exchange column (Torrence, CA, USA) was used in resolving the four diastereomers of β-methylphenylalanine standards and the enzymatic products. The β-methylphenylalanine (βMePhe) standards (Sigma-Aldrich) and enzymatic products were prepared in 1:1 $H_2O/CH_3CN$, and their chiral HPLC analyses were eluted isocratically with a $CuSO_4$ (2 mM) solution in 85:15 $H_2O/CH_3CN$.

**Table S1** Relative enzymatic activities (MT), enzyme colors and proposed functions of selected residues.

| Mutants | Relative activity[a] | Color | Function |
|---|---|---|---|
| M240L | 0.88 | turquoise | SAM/SAH binding |
| M241L | 0.91 | turquoise | SAM/SAH binding |
| M240L/M241L | 0.70 | turquoise | SAM/SAH binding |
| W99F | 0.46 | colorless | active site base |
| S104A | 0.36 | colorless | active site base |
| C136A | 0.75 | turquoise | SAM/SAH stabilization |
| C136H | 0.01 | turquoise | SAM/SAH stabilization |
| C319A | 0.61 | turquoise | allosteric regulation |
| R127L | 0.94 | yellow | Ppy binding |
| R127L/D244E | 0.70 | lime | Ppy binding/water interaction |
| R127L/D244L | 0.00 | lime | Ppy binding/water interaction |
| R127L/V300E | 0.00 | lime | hydrotase and methyltransferase |
| R127L/D244A/V300E | 0.00 | lime | hydrotase and methyltransferase |
| H243F | 0.00 | colorless | metal coordination |
| H295F | 0.01 | colorless | metal coordination |
| D244L | 0.02 | olive green | metal coordination |
| D244E | 1.20 | turquoise | metal coordination |
| V300E | 1.37 | lime | metal coordination |
| D244A/V300E | 0.26 | lime | metal coordination |
| H243D/D244H | 0.00 | colorless | metal coordination |
| H243E/D244H | 0.01 | colorless | metal coordination |
| D244H/H295D | 0.00 | colorless | metal coordination |
| D244H/H295E | 0.02 | turquoise | metal coordination |

a. The reactions of mutants were analyzed by HPLC; peak areas in triplicate were integrated and averaged; the reaction rates were calculated using the linear regression equation; relative activities were determined by dividing individual reaction rates with that of WT; the relative activity of WT is 1.0.

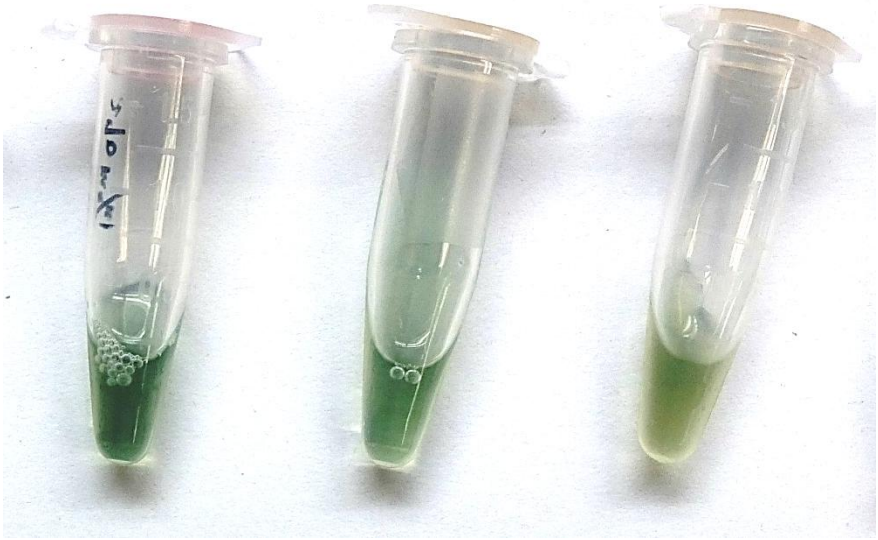


**Figure S1** Protein colors of purified MppJ and mutants thereof. The purified WT, D244E and D244L display turquoise, dark green, and olive green, respectively.

a

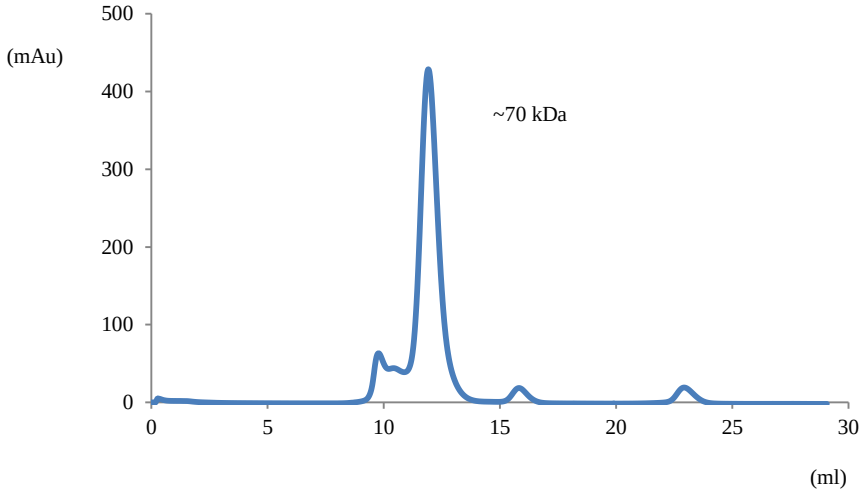


b

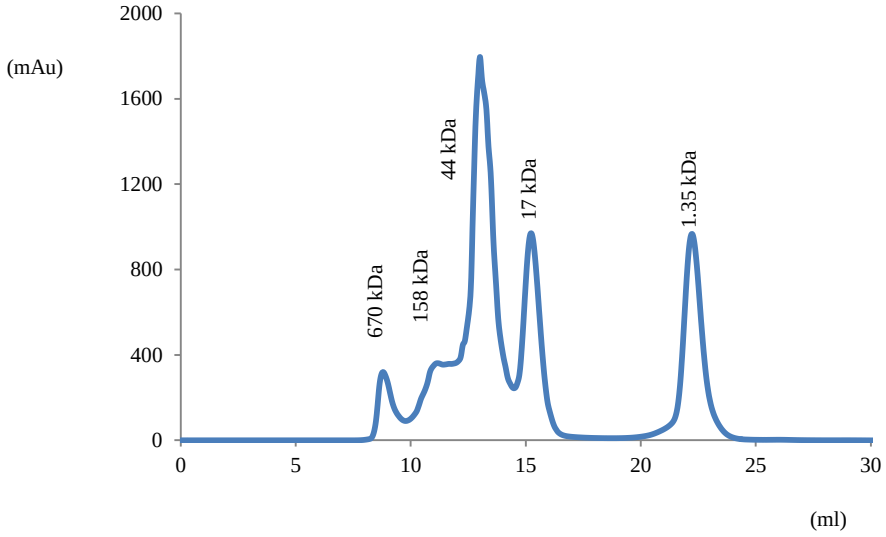


**Figure S2** Gel filtration analysis. (a) The size exclusive chromatograph of MppJ resolved by using a Superdex 75 10/300 column. (b) The size exclusive chromatograph of molecular weight standards resolved under the same condition.

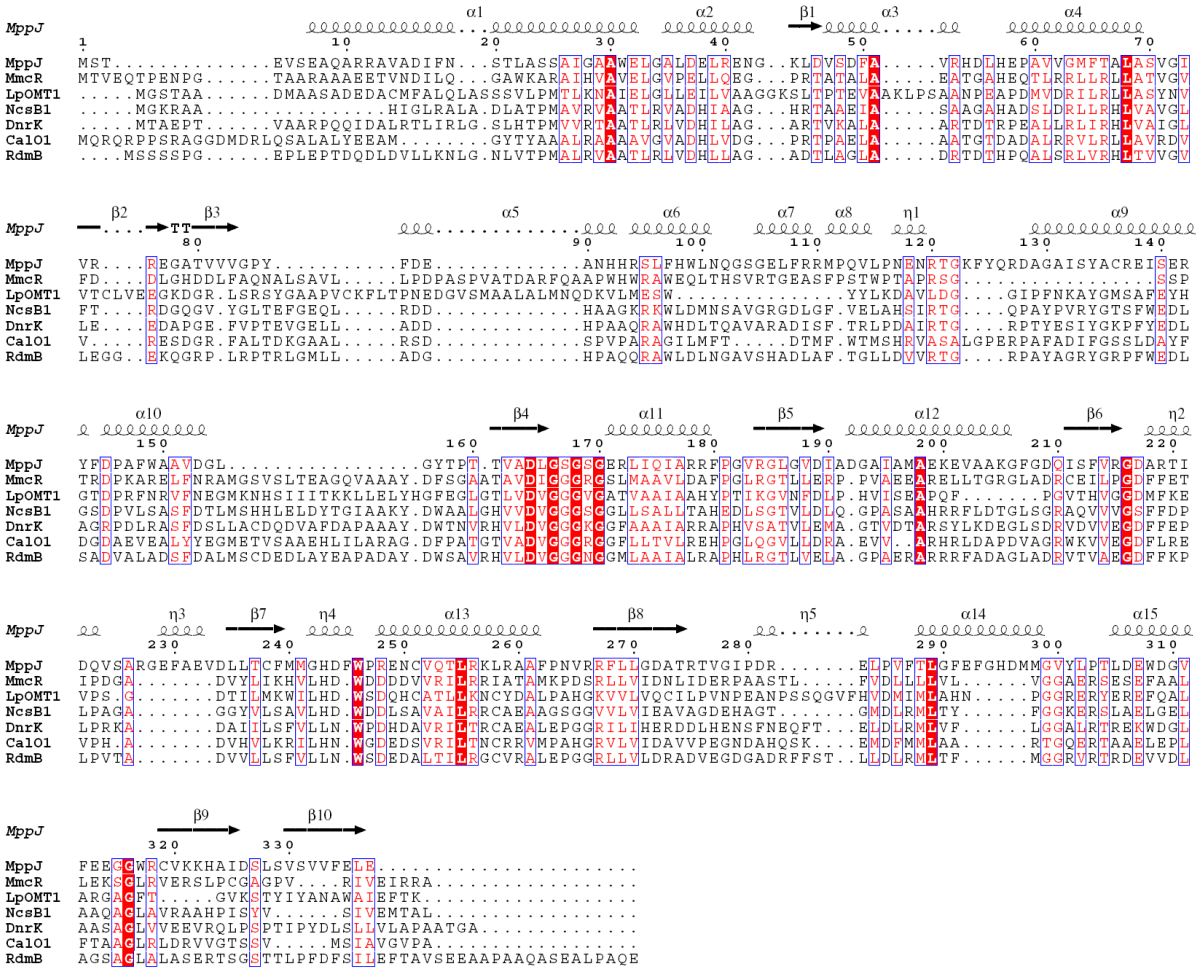


**Figure S3** Multiple sequence alignment for MppJ and homologues. The sequence alignment was performed by ClustalW (http://www.ebi.ac.uk/Tools/msa/clustalw2/). The plot was generated by ESPript (http://espript.ibcp.fr/ESPript/ESPript). The secondary structure of MppJ is shown on the top of the sequence. Accession codes for MppJ (Q643C8), MmcR (Q9X5T6), LpOMT1 (Q9ZTU2), NcsB1 (Q84HC8), DnrK (Q06528), CalO1 (Q8KNE5), and RdmB (Q54527) are designated by the UniProtKB databank (http://www.uniprot.org/).

a

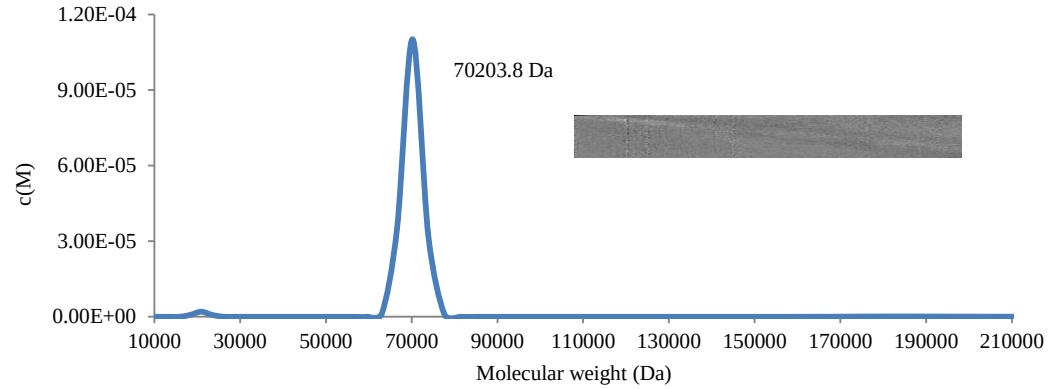


b

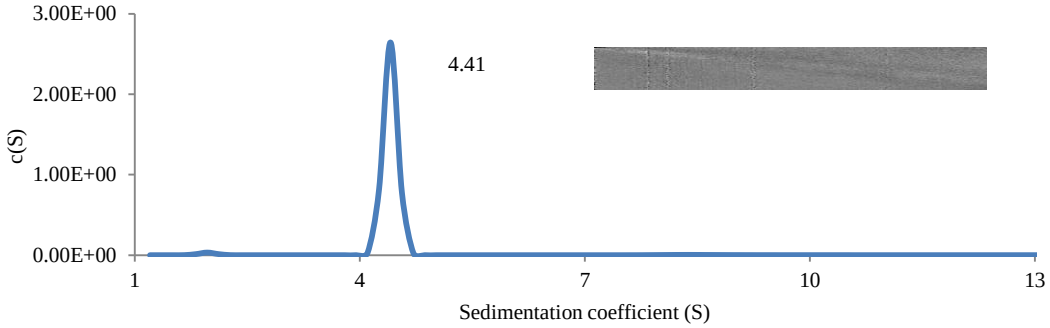


**Figure S4** Analytical ultracentrifugation analysis of MppJ. The AUC data were analyzed by SedFit (http://www.analyticalultracentrifugation.com/default.htm). The calculated *c(M)* and *c(S)* distributions are shown in the upper (a) and lower (b) panels, respectively. The insert grayscale bars indicate the residuals bitmap in each fit.

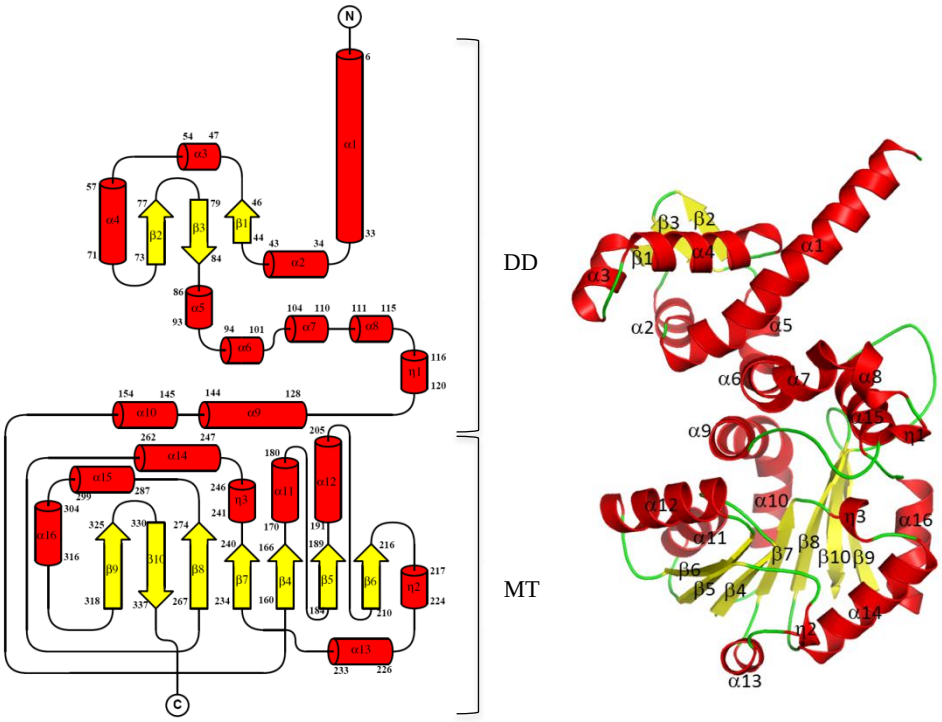


**Figure S5** Schematic topology of MppJ. The topology diagram was generated by TopDraw. The secondary structures of α-helix and β-sheet are shown in red and yellow, respectively. MppJ is composed of two domains, an N-terminal DD domain (residues 1-160) and a C-terminal MT catalytic domain (residues 161-337).

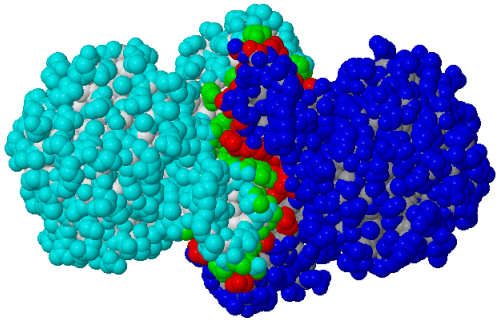

Found interfaces [XML] [View] [Details] [Download] [Search]

| ## | | Structure 1 | | | × | Structure 2 | | | interface area, Å2 | ΔiG kcal/mol | ΔiG P-value | NHB | NSB | NDS | CSS |
|---|---|---|---|---|---|---|---|---|---|---|---|---|---|---|---|
| NN | «» | Range | iNat | iNres | | Range | iNat | iNres | | | | | | | |
| 1 | ◉ | A | 344 | 80 | ◊ | B | 340 | 79 | 3135.0 | -45.4 | 0.003 | 23 | 8 | 0 | 0.000 |

[View] [Details] [Download] [Search] Viewer: Jmol

interface #1/1 [XML] [<<] [<] [>] [>>]

**interface Summary** [XML]

| | Structure 1 | Structure 2 |
|---|---|---|
| **Selection range** | A | B |
| **Class** | Protein | Protein |
| **Symmetry operation** | x,y,z | ,, |
| **Symmetry ID** | 1_555 | 0_555 |
| **Number of atoms** | | |
| interface | 344 (13.3%) | 340 (13.2%) |
| surface | 1488 (57.6%) | 1450 (56.1%) |
| total | 2585 (100.0%) | 2585 (100.0%) |
| **Number of residues** | | |
| interface | 80 (24.1%) | 79 (23.8%) |
| surface | 307 (92.5%) | 301 (90.7%) |
| total | 332 (100.0%) | 332 (100.0%) |
| **Solvent-accessible area, A2** | | |
| interface | 3127.2 (19.6%) | 3142.9 (19.9%) |
| total | 15929.1 (100.0%) | 15768.7 (100.0%) |
| **Solvation energy, kcal/mol** | | |
| isolated structure | -297.3 (100.0%) | -295.3 (100.0%) |
| gain at complex formation | -22.6 (7.6%) | -22.8 (7.7%) |
| average gain | -7.7 (2.6%) | -8.4 (2.8%) |
| P-value | 0.003 | 0.004 |

**Hydrogen bonds** [XML]

| ## | Structure 1 | Dist. [A] | Structure 2 |
|---|---|---|---|
| 1 | A:GLN 113[ NE2] | 3.07 | B:GLU 32[ OE2] |
| 2 | A:ASN 117[ N ] | 3.01 | B:ASP 55[ O ] |
| 3 | A:ARG 109[ NH1] | 3.07 | B:GLN 102[ O ] |
| 4 | A:SER 25[ OG ] | 3.00 | B:PHE 108[ O ] |
| 5 | A:GLN 102[ NE2] | 2.79 | B:ARG 109[ O ] |
| 6 | A:HIS 57[ N ] | 2.91 | B:LEU 115[ O ] |
| 7 | A:ARG 109[ NH1] | 3.68 | B:ASP 128[ OD2] |
| 8 | A:ARG 76[ NH1] | 2.84 | B:ASP 281[ OD1] |
| 9 | A:ARG 76[ NH1] | 2.90 | B:ASP 281[ OD2] |
| 10 | A:ASN 19[ ND2] | 3.34 | B:LEU 284[ O ] |
| 11 | A:ARG 12[ NH2] | 2.77 | B:LEU 284[ O ] |
| 12 | A:GLU 32[ OE2] | 3.08 | B:GLN 113[ NE2] |
| 13 | A:ASP 55[ O ] | 2.90 | B:ASN 117[ N ] |
| 14 | A:SER 70[ O ] | 3.25 | B:ARG 282[ NE ] |
| 15 | A:GLN 102[ O ] | 2.69 | B:ARG 109[ NH1] |
| 16 | A:PHE 108[ O ] | 3.83 | B:GLN 102[ NE2] |
| 17 | A:PHE 108[ O ] | 2.84 | B:SER 25[ OG ] |
| 18 | A:ARG 109[ O ] | 2.94 | B:GLN 102[ NE2] |
| 19 | A:LEU 115[ O ] | 2.89 | B:HIS 57[ N ] |
| 20 | A:ASP 128[ OD2] | 3.36 | B:ARG 109[ NH1] |
| 21 | A:ASP 281[ OD1] | 2.63 | B:ARG 76[ NH1] |
| 22 | A:LEU 284[ O ] | 3.37 | B:ASN 19[ ND2] |
| 23 | A:LEU 284[ O ] | 3.12 | B:ARG 12[ NH2] |

**Salt bridges** [XML]

| ## | Structure 1 | Dist. [A] | Structure 2 |
|---|---|---|---|
| 1 | A:ARG 109[ NH1] | 3.68 | B:ASP 128[ OD2] |
| 2 | A:ARG 76[ NH1] | 2.84 | B:ASP 281[ OD1] |
| 3 | A:ARG 76[ NE ] | 3.68 | B:ASP 281[ OD2] |
| 4 | A:ARG 76[ NH1] | 2.90 | B:ASP 281[ OD2] |
| 5 | A:ASP 128[ OD2] | 3.36 | B:ARG 109[ NH1] |
| 6 | A:ASP 281[ OD1] | 2.63 | B:ARG 76[ NH1] |
| 7 | A:ASP 281[ OD2] | 3.88 | B:ARG 76[ NE ] |
| 8 | A:ASP 281[ OD2] | 3.06 | B:ARG 76[ NH1] |

**Figure S6** Interfaces analysis of MppJ. PISA (Krissinel & Henrick, 2007) analysis showed that the interfaced area of an MppJ dimer is 3135 Å$^2$, mainly dominated by hydrophobic interactions, 23 hydrogen bonds and 8 salt bridges. The analysis statistics is demonstrated on the bottom panel.

a

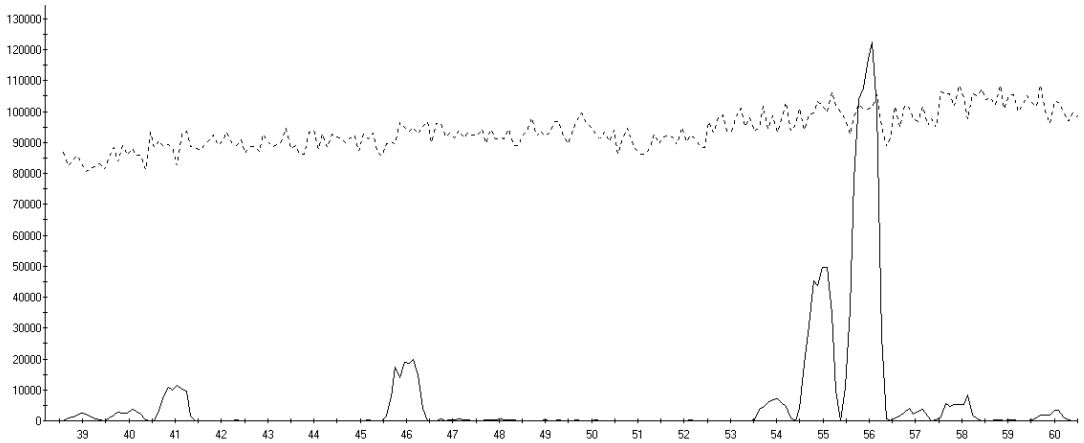


b

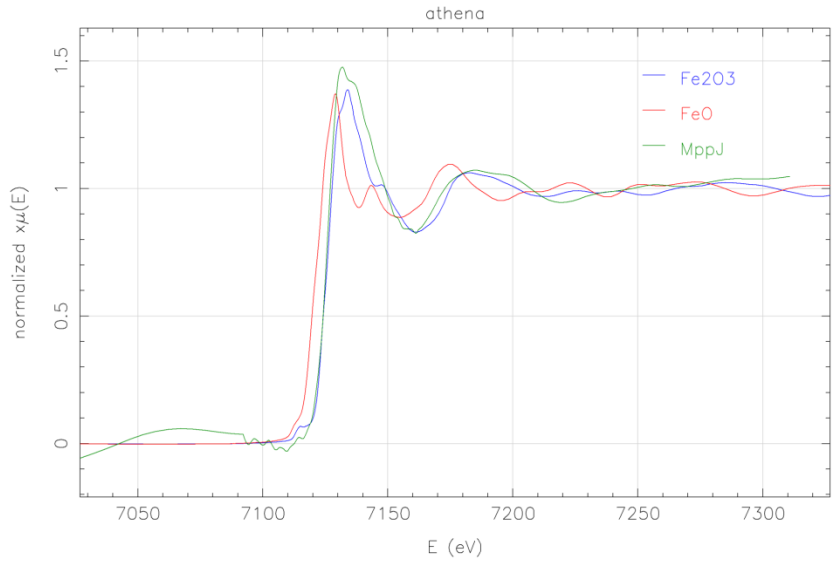


**Figure S7** Metal ion determination by inductively coupled plasma mass spectrometry (ICP-MS) and X-ray absorption spectroscopy (XAS). (a) The ICP-MS spectrum (the molecular weight of Fe is 56 a.m.u.) (b) The XAS spectra, wherein MppJ, $Fe^{3+}$ and $Fe^{2+}$ are colored in green, blue and red, respectively.

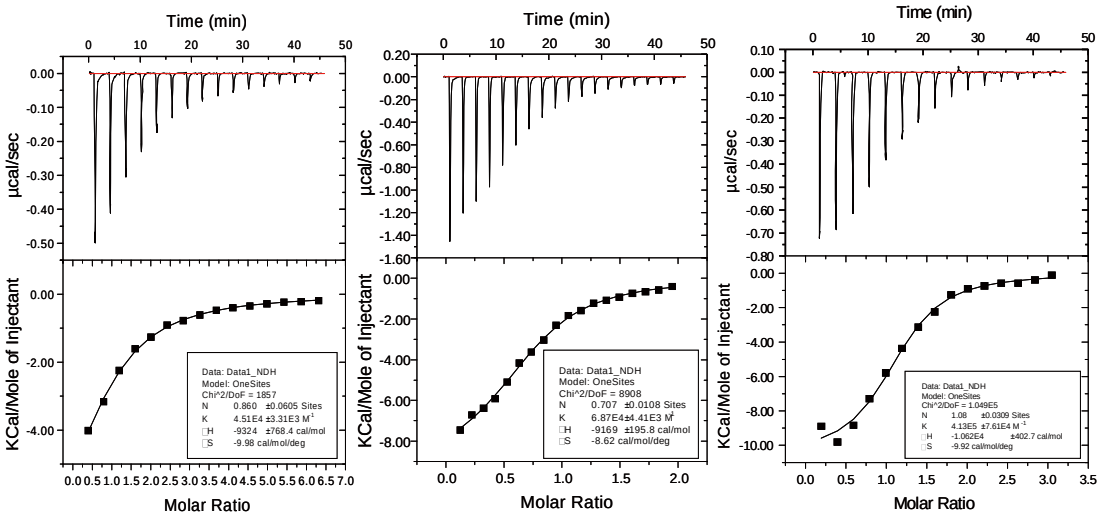


MppJ-SAM ($K_d$=22.4±1.6 µM) MppJ-Ppy ($K_d$=14.6±0.9 µM) MppJ-SAH ($K_d$=2.5±0.4 µM)

**Figure S8** Isothermal titration calorimetry (ITC) analysis of MppJ. The ITC thermograms of MppJ versus SAM, Ppy, or SAH. Each exothermic heat pulse corresponds to an injection of 2 µl of ligands (1 mM) into the protein solution (0.1 mM); integrated heat areas constitute a differential binding curve that was fitted with a standard single-site binding model (Origin 7.0, MicroCal iTC200).

a b

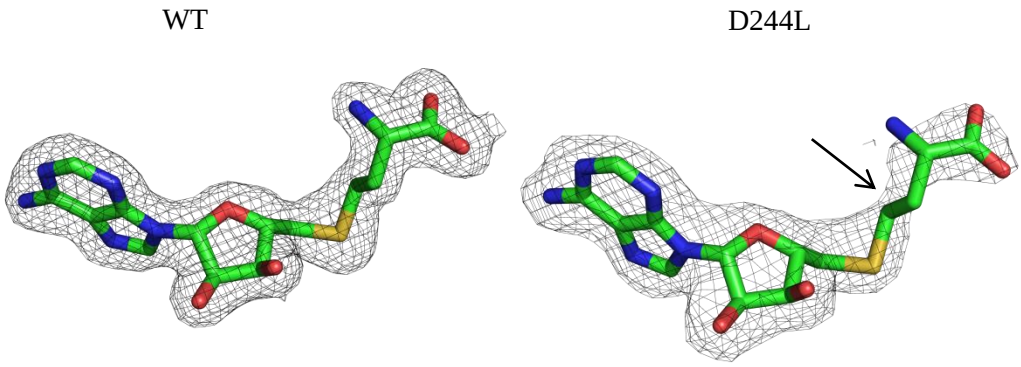


**Figure S9** Structure and electron density map of SAH in WT and D244L mutant. (a) The $2F_o$-$F_c$ electron density map of SAH in WT. (b) The $2F_o$-$F_c$ electron density map of SAH in D244L mutant, where the bond between the sulfur atom and 2-aminobutanoic acid is partially discontinued.

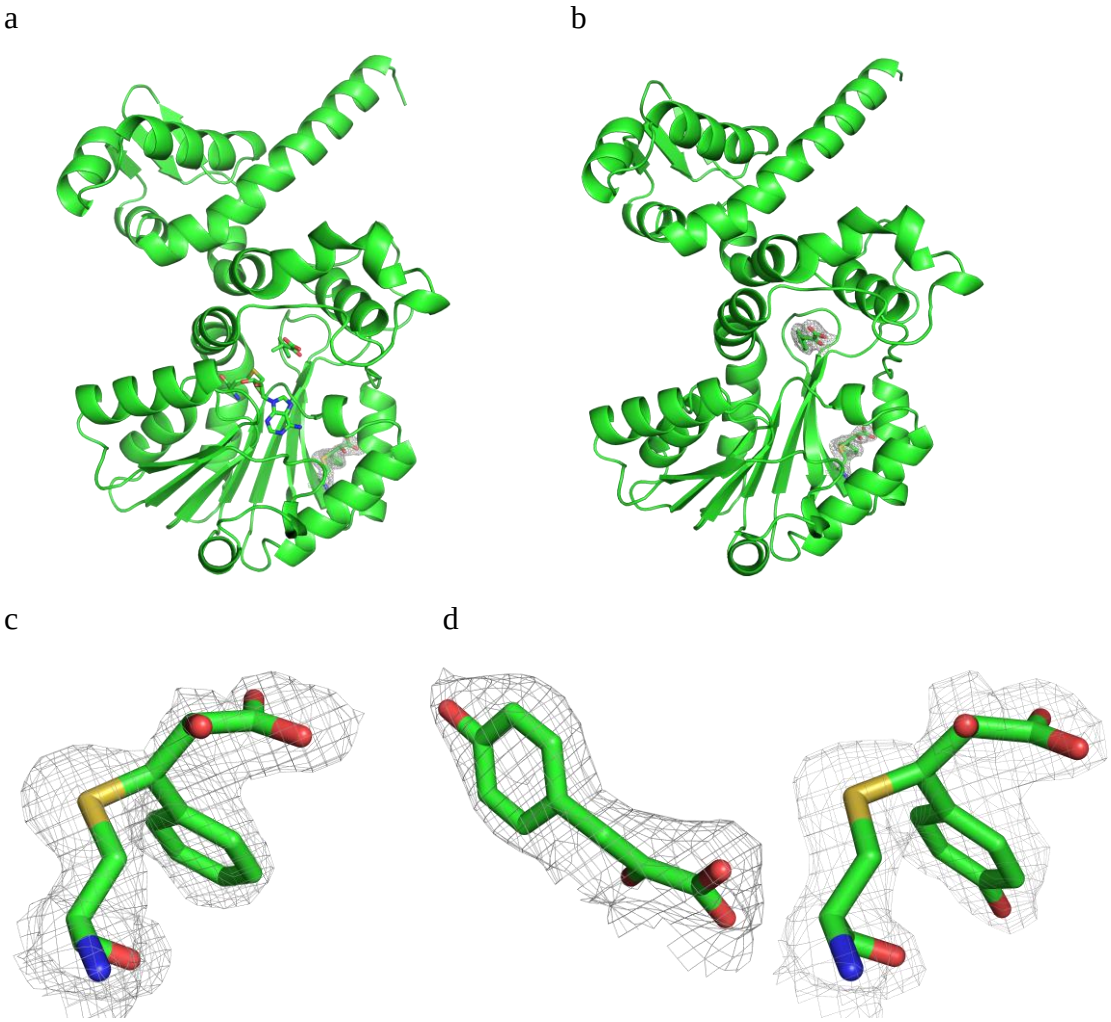


**Figure S10** Ppy/4HPpy are covalently linked to Cys319. (a) The structure of the MppJ-SAH-MePpy complex. (b) The structure of the MppJ-4HPpy complex. (c) The $2F_o$-$F_c$ electron density map of the covalently linked Ppy contoured at 1 σ. (d) The $2F_o$-$F_c$ electron density maps of the active site 4HPpy and the covalently linked 4HPpy contoured at 1 σ.

a.

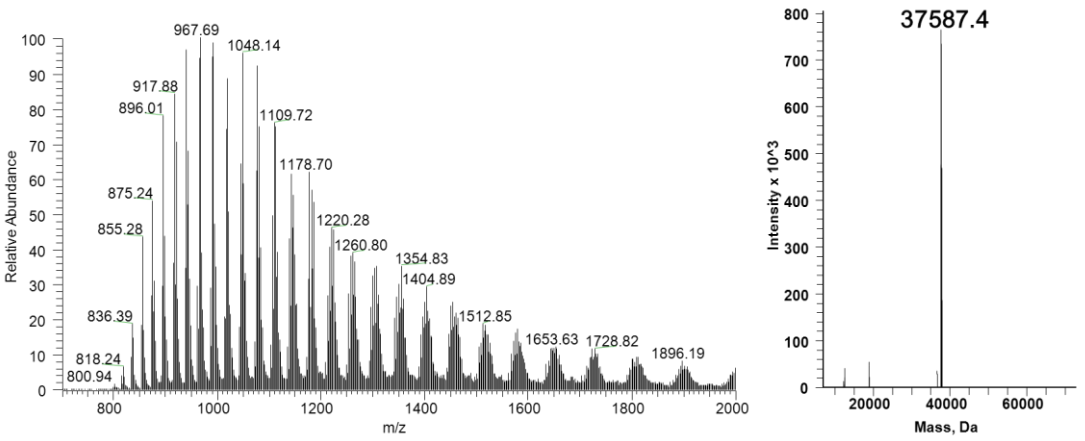


b.

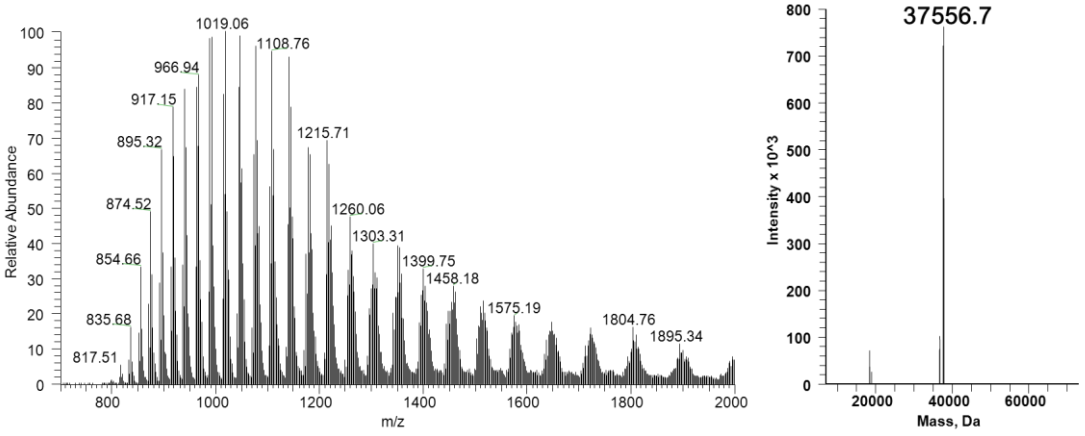


c.

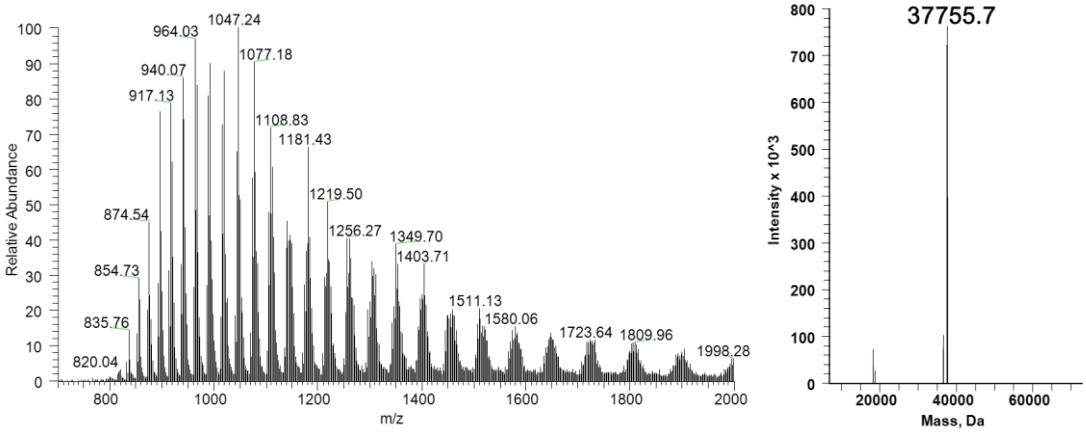


**Figure S11** Mass spectrometric analysis of MppJ and mutant thereof. (a) The mass spectrum of WT (left panel) and the corresponding de-convoluted mass (right panel) in the absence of Ppy. (b) The mass spectrum of C319A (left panel) and the corresponding de-convoluted mass (right panel) in the presence of Ppy. (c) The mass spectrum of WT (left panel) and the corresponding de-convoluted mass

(right panel) in the presence of Ppy. The protein mass of WT in the presence of Ppy gains additional mass units (Δ168 amu ~ Ppy) relative to that of WT in the absence of Ppy, as opposed to that of C319A which losses 30 amu (equivalent to a sulfur atom), confirming that Ppy is covalently linked to the residue C319 of MppJ.

### Supporting references

Krissinel, E. & Henrick, K. (2007). *J. Mol. Biol.* **372**, 774-797.
Ravel, B. & Newville, M. (2005). *Journal of Synchrotron Radiation* **12**, 537-541.
Schuck, P. (2000). *Biophys. J.* **78**, 1606-1619.